# The stellar contribution to the extra-galactic background light and absorption of high-energy gamma-rays

Soebur Razzaque[1,2], Charles D. Dermer[1] and Justin D. Finke[1,2]


## ABSTRACT

TeV $\gamma$ rays from distant astrophysical sources are attenuated due to electron-positron pair creation by interacting with ultraviolet/optical to infrared photons which fill the universe and are collectively known as the extra-galactic background light (EBL). We model the $\sim$0.1–10 eV starlight component of the EBL derived from expressions for the stellar initial mass function, star formation history of the universe, and wavelength-dependent absorption of a large sample of galaxies in the local universe. These models are simultaneously fitted to the EBL data as well as to the data on the stellar luminosity density in our local universe. We find that the models with modified Salpeter A initial mass function together with Cole et al. (2001) or Hopkins & Beacom (2006) star formation history best represent available data. Since no dust emission is included, our calculated EBL models can be interpreted as the lower limits in the $\sim$0.1–1 eV range. We present simple analytic fits to the best-fit EBL model evolving with redshift. We then proceed to calculate $\gamma$-ray opacities, and absorption of $\sim$10–300 GeV $\gamma$-rays coming from different redshifts. We discuss implications of our results for the Fermi Gamma Ray Space Telescope and ground-based Air Cherenkov Telescopes.


*Subject headings:* stars: formation—stars: fundamental parameters—stars: luminosity function, mass function—dust, extinction—diffuse radiation—gamma rays: observations

## 1. Introduction

Stars are the dominant sources of electromagnetic radiation in the universe after the cosmic microwave background (see, e.g., Fukugita & Peebles 2004). They emit radiation

[1]Space Science Division, Code 7653, U.S. Naval Research Laboratory, Washington, DC 20375; srazzaque@ssd5.nrl.navy.mil

[2]National Research Council Research Associate

longward from ultraviolet to infrared wavelengths. However, photons with wavelength $\lesssim$ 2 $\mu$m are highly absorbed by the dust in the host galaxies and only a fraction of the radiation emitted by the stars escape to the inter-galactic medium and form a diffuse background or EBL (see, e.g., Baldry & Glazebrook 2003; Driver et al. 2008). The dust in the host galaxies, heated by the starlight, also radiate in the infrared wavelengths and contribute to the EBL density at $\sim 10^{12}$ Hz. It is the direct starlight component, $\lesssim 2$ $\mu$m or $\gtrsim 0.1$ eV, that affects the propagation of $\lesssim 5$ TeV $\gamma$-rays from distant sources. Indeed, the very soft spectral energy distribution ($dN/dE \propto E^{-\Gamma}$) with $\Gamma \gtrsim 3$ observed from several TeV blazars at high redshift ($z \gtrsim 0.1$) such as PKS 2155-304 (Aharonian et al. 2005), H 2356-309 (Aharonian et al. 2006a); 1ES 1218+304 (Albert et al. 2006); 1ES 1101-232 (Aharonian et al. 2006b); 0347-121 (Aharonian et al. 2007), 1ES 1011+496 (Albert et al. 2007) and 3C 279 (Albert et al. 2008), and their cutoff at $\gtrsim 1$ TeV are hints that high energy $\gamma$ rays from these sources are absorbed by the EBL UV/optical photons (Persic & de Angelis 2008). Lower energy (<TeV) $\gamma$-rays from high redshift sources such as gamma-ray bursts (GRBs) and blazars can also probe the EBL starlight component.

Calculation of the opacity of the universe to $\gamma$-rays by $\gamma\gamma \rightarrow e^+e^-$ process dates back to Nishikov (1961), followed by Gould & Shréder (1966) and Fazio & Stecker (1970). More recently Malkan & Stecker (1998, 2001); Primack et al. (1999); Kneiske, Mannheim & Hartmann (2002); Kneiske et al. (2004); Primack, Bullock and Somerville (2005); Stecker, Malkan & Scully (2006) calculated EBL models adopting either a phenomenological approach or Monte Carlo galaxy formation code. These models trace the general trend of the data, which may be fitted with a combination of two or more modified blackbody spectra for its two distinct peaks at the infrared and optical wavebands (Dermer 2007). Significant uncertainty in data and large dispersion among models led to an indirect method to constrain the EBL, namely by estimating change in spectral slope from distant TeV blazars due to $\gamma\gamma$ absorption (Stecker & de Jager 1993; Stanev & Franceschini 1998; Mazin & Raue 2007). However, such a method generally does not include possible absorption at the source (see, e.g., Reimer 2007) and presumes a source spectrum.

In this paper, we build models of the EBL starlight component ($\sim$0.1–10 eV) directly from the stellar thermal surface radiation. Emission from an individual star during its main-sequence lifetime is well approximated as a blackbody with a mass-dependent temperature. The post-main-sequence lifetime of a star is very short compared to its main-sequence lifetime and their contribution at the UV-optical wave bands is not significant. They can, however, contribute significantly to longer wavelengths due to their increased luminosity in the post-main-sequence phase (Finke et al., in preparation). Only a small fraction of the stars with mass $\gtrsim 8M_\odot$ produce supernovae and even a smaller fraction produce GRBs. Emission from these sources dominate the diffuse MeV background (Watanabe et al. 1999; Ruiz-Lapuente,

Cassé & Vangioni-Flam 2001; see, however, Strigari et al. 2005; Inoue, Totani & Ueda 2008). Emission from quasars and AGNs, on the other hand, dominate the diffuse X-ray background (Mushotzky et al. 2000). Contributions from all these sources add only a small fraction to the total cosmic electromagnetic energy density in the $\sim 0.1$–10 eV range, and we also ignore that. The estimated lifetimes of individual stars depend on their masses and the assumed cosmology, which is the standard $\Lambda$CDM with $(h,\ \Omega_m,\ \Omega_\Lambda) = (0.7, 0.3, 0.7)$, and the Hubble constant $H_0 = 70h_{0.7}$ km s$^{-1}$ Mpc$^{-1}$. Summing over contributions from stars of all masses formed in the history of the universe then gives us the diffuse emission or EBL.

A sum over contributions from individual stars radiating at a given redshift corresponds to the luminosity density or the stellar energy emissivity of the universe at that redshift. The initial mass function (IMF), which is the distribution of stars by mass, and the star formation rate (SFR), which is the mass that forms stars per unit comoving volume per unit time, are two uncertain but related parameters in our calculation. We form classes of models by choosing different combinations of these parameters and compare, in the UV-optical band, the luminosity density data of the local universe found from the surveys of nearby galaxies. The same models are then compared with EBL data. Note that there are no adjustable free parameters in our calculation once we choose a particular model.

Finally we use one of our best-fit models to calculate the $e^{\pm}$ pair production opacities in the $\sim$10–300 GeV energy range at different redshifts. These results are applicable to high-energy emission from distant sources such as GRBs and blazars detected by the currently operating Fermi Gamma Ray Space Telescope and Air Cherenkov Telescopes such as HESS, MAGIC and VERITAS.

In Sec. 2 we outline the formalism of our method and introduce different models in Sec. 3 upon which we base our EBL calculation. We report our results in Sec. 4, compare with results from previous authors as well as calculate EBL evolution with redshift. We discuss implications of our results for $\gamma$-ray astronomy in Sec. 5, calculating $\gamma\gamma \to e^+e^-$ absorption opacity ($\tau_{\gamma\gamma}$) for high energy $\gamma$ rays from sources at different redshifts. Conclusions of the work for EBL and $\gamma$ ray absorption are given in Sec. 6.

## 2. Formalism

The differential number density (per unit volume) of thermal blackbody photons in the energy interval $\epsilon$ to $\epsilon + d\epsilon$ at a given temperature $T$ is

$$\frac{dN}{d\epsilon dV} = \frac{1}{\pi^2(\hbar c)^3}\frac{\epsilon^2}{\exp(\epsilon/kT) - 1} \tag{1}$$

and the total number of photons emitted per unit energy and time intervals from a star of radius $R$ is given by

$$\frac{dN(\epsilon, M)}{d\epsilon dt} \;=\; \pi R^2 c \, \frac{dN}{d\epsilon dV} \; . \tag{2}$$

The radius and temperature of a star depend on its mass $M$, and can be calculated in terms of the solar radius $R_\odot$, mass $M_\odot$ and temperature $T_\odot$ using various relations. We use a fit to the stellar mass-radius relation (Schmidt-Kaler 1982; Binney & Merrifield 1998) as

$$R/R_\odot = \begin{cases} (M/M_\odot)^{0.8} \; ; \; 0.1M_\odot \leq M \leq 10M_\odot \\ 10^{9/20}(M/M_\odot)^{0.35} \; ; \; 10M_\odot < M \leq 120M_\odot \; . \end{cases} \tag{3}$$

The stellar mass-luminosity ratio is not well-known. To the first approximation, it is a single power law (SPL), given by

$$L/L_\odot = (M/M_\odot)^{3.6} \; . \tag{4}$$

A more detailed relation is calculated by Bressan et al. (1993) and a simple broken power law (BPL) fit to that relation (Binney & Merrifield 1998) is given by

$$L/L_\odot = f_L \begin{cases} (M/M_\odot)^{4.8} \; ; \; M < 2M_\odot \\ 2^{13/10}(M/M_\odot)^{3.5} \; ; \; 2M_\odot \leq M \leq 20M_\odot \\ 2^{201/50}5^{34/25}(M/M_\odot)^{2.14} \; ; \; M > 20M_\odot \; . \end{cases} \tag{5}$$

Although there are uncertainties, depending on the metallicity e.g., in the mass-to-light ratio, we assume $f_L = 1$ for our modeling purposes. Stars below $1M_\odot$ and above $20M_\odot$, in the Bressan et al. (1993) model, produce much less light than the model with a single power-law [equation (4)] for the same masses. We derive a stellar mass-temperature relation from the luminosity $L = 4\pi R^2 \sigma T^4$, where $\sigma$ is the Stefan-Boltzmann constant. For the SPL relation in equation (4) between $L - M$, the temperature is

$$T/T_\odot = \begin{cases} (M/M_\odot)^{1/2} \; ; \; M \leq 10M_\odot \\ 10^{-9/40}(M/M_\odot)^{0.725} \; ; \; M > 10M_\odot \; , \end{cases} \tag{6}$$

following the break in equation (3). For the BPL relation of $L - M$ in equation (5), the $T - M$ relation is

$$T/T_\odot \;=\; f_L^{1/4} \begin{cases} (M/M_\odot)^{0.8} \; ; \; 0.1M_\odot \leq M < 2M_\odot \\ 2^{13/40}(M/M_\odot)^{0.475} \; ; \; 2M_\odot \leq M \leq 10M_\odot \\ 2^{1/10}5^{-9/40}(M/M_\odot)^{0.7} \; ; \; 10M_\odot < M \leq 20M_\odot \\ 2^{39/50}5^{23/200}(M/M_\odot)^{0.36} \; ; \; M > 20M_\odot \; . \end{cases} \tag{7}$$

For reference, $M_\odot = 1.99 \times 10^{33}$ g, $L_\odot = 3.846 \times 10^{33}$ ergs s$^{-1}$ and $T_\odot = 5777$ K are solar mass, luminosity, and temperature respectively.

One needs to take cosmology into account to calculate the total number of photons emitted from a star over cosmic time which was born at a past epoch. The relationship between the cosmic time and redshift is given by

$$(dt/dz)^{-1} = -H_0(1+z)\sqrt{\Omega_m(1+z)^3 + \Omega_\Lambda}\ . \tag{8}$$

The main sequence lifetime of a star with mass $M$ is

$$t_\star \approx t_\odot (M/M_\odot)/(L/L_\odot)\ , \tag{9}$$

where $t_\odot \approx 11$ Gyr is the lifetime of the Sun. If a star of mass $M$ was born at a redshift $z$ then the redshift $z_{\rm d}(M)$ at which it had evolved off the main sequence can be found from the inverse of the relation $t_\star(M) = \int_{z_{\rm d}(M)}^{z} dz'\,|dt/dz'|$ as

$$z_{\rm d}(M,z) = -1 + \Bigg(-(\Omega_\Lambda/\Omega_m)\ {\rm sech}\left[(3/2)H_0 t_\star\sqrt{\Omega_\Lambda} + \tanh^{-1}\sqrt{1+(\Omega_m/\Omega_\Lambda)(1+z)^3}\right]^2\Bigg)^{1/3}\ , \tag{10}$$

We have plotted this redshift in Fig. 1 for different $M$ and $z$ and setting it equal to zero if $z_{\rm d}(M) < 0$. After calculating $z_{\rm d}$ for a given $(z, M)$ combination, we back-calculate $z$ as a check. The results are identical. Note that high mass stars $\gtrsim 10M_\odot$ evolve off the main sequence almost at the same redshift ($z \approx 1$ – 5) they were formed. On the contrary, a star with mass $\sim 1M_\odot$ lives almost a Hubble time. Note that $z_{\rm d}$, following $t_\star$, depends on the $L - M$ relation. For the curves in Fig. 1 we used both the SPL (dashed lines) and BPL (dotted lines) $L - M$ relations given, respectively, by equations (4) and (5).

Equation (9) represents an underlying source of uncertainty for high-mass stars and/or high redshift stars. Our naive estimate of stellar lifetime and luminosity are based on the model of the Sun, and assuming that stars are perfect blackbodies. Estimates of the Sun's age are based on the total amount of fusion material ($4{\rm H}^+ \rightarrow {\rm He}^{++}$) in the core. This amounts to about 10% of the Sun's mass. The estimates for high mass stars or stars with different metallicities are less precise. High mass stars often have winds which may reduce their net radiative output, however, they can also be approximated as perfect blackbodies because of their higly ionized surface. Since the fraction of high-mass stars is small, we neglect corrections to equation (9) in this study.

The integrated number of photons emitted by a star from its birth at redshift $z$ to the present epoch, in the energy interval $d\epsilon = d\epsilon'/(1+z')$, can be calculated using equations (2),

(3), (4) or (5), (6) or (7) and (10) as

$$\frac{dN(\epsilon,M)}{d\epsilon}=\int_{\max\{0,\ z_{\rm d}(M,z')\}}^{z}dz'\left|\frac{dt}{dz'}\right|\frac{dN(\epsilon',M)}{d\epsilon' dt}(1+z')\ , \tag{11}$$

where the lower limit of the integration is set to zero if the star has survived to the present epoch.

The number of stars formed at a redshift $z$ depends on the initial mass function and star formation rate, both of which are important sources of uncertainty in our calculation and are discussed shortly. We assume a universal IMF which is normalized between mass $(M_{\rm min}$ – $M_{\rm max})=(0.1$ – $120)M_\odot$ as $\mathcal{N}^{-1}=\int_{M_{\rm min}}^{M_{\rm max}}dM(dN/dM)M$. The final number of photons reaching us from all stars created in the past, per unit energy interval, amounts to weighting equation (11) by the normalized IMF, $\mathcal{N}(dN/dM)$, and integrating over stellar mass (to take into account photons created by stars of all mass) and, after weighting by the SFR $\psi(z)$ in units of $M_\odot$ yr$^{-1}$ Mpc$^{-3}$, integrating over redshift $z$ (to take into account stars created at all epochs). The spectral stellar radiation density is therefore given by

$$\begin{aligned}\frac{dN(\epsilon,z=0)}{d\epsilon dV}&=\mathcal{N}\int_{z=0}^{\infty}dz''\left|\frac{dt}{dz''}\right|\psi(z'')\int_{M_{\rm min}}^{M_{\rm max}}dM\left(\frac{dN}{dM}\right)\\&\times\int_{\max\{0,\ z_{\rm d}(M,z')\}}^{z''}dz'\left|\frac{dt}{dz'}\right|f_{\rm esc}(\epsilon')\frac{dN(\epsilon',M)}{d\epsilon' dt}(1+z').\end{aligned} \tag{12}$$

Here $dN(\epsilon',M)/d\epsilon' dt$ is given by equation (2) with the substituton $\epsilon'=\epsilon(1+z')$, and $f_{\rm esc}(\epsilon')$ is the escape fraction of photons from the host galaxy, considered further in the next section. Note that there is no free parameters in our model once we chose particular models of SFR, IMF and $L-M$ relation.

Equation (12) can be converted to the EBL energy density $\epsilon u_\epsilon$ (e.g., in units of ergs cm$^{-3}$) by multiplying with $\epsilon^2$ or to intensity $\epsilon I_\epsilon$ (e.g., in units of W m$^{-2}$ sr$^{-1}$) by multiplying with $\epsilon^2 c/4\pi$. The differential photon number density in equation (12) or EBL energy density measured at present from a past epoch ($z=z_1$) can be transformed to the past epoch, i.e. comoving EBL density, with $\epsilon_1=\epsilon(1+z_1)$ and the comoving volume $V_1=V/(1+z_1)^3$ as

$$\begin{aligned}\frac{dN(\epsilon_1,z_1)}{d\epsilon_1 dV_1}&=(1+z_1)^2\frac{dN(\epsilon,z=z_1)}{d\epsilon dV}\\ \epsilon_1 u_{\epsilon_1}&=(1+z_1)^4\epsilon^2\frac{dN(\epsilon,z=z_1)}{d\epsilon dV}.\end{aligned} \tag{13}$$

Note that we use $z=z_1$ as the lower limit of the outer integration over redshift in equation (12) to calculate $dN(\epsilon,z=z_1)/d\epsilon dV$.

### 2.1. Energy output by the local universe

The cosmic energy output or luminosity density $\epsilon L_\epsilon$ (e.g. in units of W Mpc$^{-3}$) in starlight is generally found from the galaxy counts in the local universe (see, e.g., Baldry & Glazebrook 2003; Driver et al. 2008). This is equivalent to summing over energy output by individual stars which were born at a past epoch but still radiating today ($z = z_1 \approx 0$), and we calculate the comoving luminosity density by modifying equation (12) as

$$\begin{aligned} \epsilon_1 L_{\epsilon_1} &= \epsilon^2 (1+z_1)^5 \mathcal{N} f_{\rm esc}(\epsilon_1) \int_{M_{\rm min}}^{M_{\rm max}} dM \left(\frac{dN}{dM}\right) \frac{dN(\epsilon_1, M)}{d\epsilon_1 dt} \\ &\times \int_{z_1 \approx 0}^{z_{\rm b}(M,z_1)} dz'' \left|\frac{dt}{dz''}\right| \psi(z'') \ . \end{aligned} \tag{14}$$

Here $z_{\rm b}(M, z_1)$ is the maximum redshift a star may born, within comoving Hubble time $1/H_0(1+z_1)$, to contribute to the local power depending on its mass. This can be calculated from equation (10) by switching the sign of the second term inside the square brackets.

Note that an integration of the luminosity density, the comoving quantity in equation (14) divided by $(1+z_1)^4$ and multiplying with it after integration, over cosmic time also leads to the comoving EBL energy density, an approach advocated by Salamon & Stecker (1998) and by Dwek et al. (1998). This amounts to adding up luminosity densities from all past epochs measured at a particular epoch to calculate the EBL. Both this approach and our formalism given by equations (12) & (13) produce the same EBL result as we have tested at different redshifts.

## 3. Models of Star formation and dust attenuation

The star formation history of the universe and the number of stars formed at a given epoch are not independent. A combination of both are needed to fit the SFR data (see, e.g., Madau et al. 1996; Cole et al. 2001; Hopkins & Beacom 2006) and the luminosity density data from local galaxy surveys (see, e.g., Baldry & Glazebrook 2003; Driver et al. 2008). The classic Salpeter (1955) IMF is still preferred by astronomers with some modifications. The modified "Salpeter A" model IMF is $dN/dM \propto M^{-\kappa}$ with $\kappa = 1.5$ below $0.5M_\odot$ and 2.35 above $0.5M_\odot$. Models by Scalo (1986; 1998) are in violation with a strong upper limit of $\kappa < 2.7$ above $1M_\odot$ as found by Baldry & Glazebrook (2003). We also use the "Baldry-Glazebrook" IMF model with $\kappa = 1.5$ below $0.5M_\odot$ and $\kappa = 2.2$ above $0.5M_\odot$.

Cole et al. (2001) found a parametric form of the SFR given by $\psi(z) = h(a+bz)/[1 + (z/c)^d]$, with parameters $(a, b, c, d) = (0.0166, 0.1848, 1.9474, 2.6316)$. Hopkins & Beacom

(2006) also used this parametric form, as well as their own piecewise fit in the form $\sim 10^{a'}(1+z)^{b'}$, along with the "Salpeter A" and "Baldry-Glazebrook" IMF to fit SFR data. The best-fit parameters they found are given in their Tables 1 and 2. We define five models of different IMF and SFR combinations as:

- *Model A:* Cole et al. (2001) SFR and Salpeter A IMF
- *Model B:* Cole et al. (2001) SFR formula fitted by Hopkins & Beacom (2006) with Salpeter A IMF
- *Model C:* Cole et al. (2001) SFR formula fitted by Hopkins & Beacom (2006) with Baldry-Glazebrook IMF
- *Model D:* Hopkins & Beacom (2006) SFR with Salpeter A IMF
- *Model E:* Hopkins & Beacom (2006) SFR with Baldry-Glazebrook IMF

We plot these models in Fig. 3. Note that there is a significant amount of uncertainty among the models even at $z \sim 0$. Also, at the highest redshifts the SFR models may be underestimating the true rate (see, e.g., Faucher-Giguère et al. 2008). Most of the uncertainty comes from the dust in the host galaxies that absorbs stellar emission and reemits it into infrared wavebands, forming the low energy, $< 0.1$ eV, part of the EBL. A precise model of the fraction of starlight which directly escapes the host galaxy is still missing. Such a model would depend on the galaxy types and their orientations as well as on redshift.

Bearing in mind the uncertainties in dust absorption models discussed above, we adopt a model recently developed by Driver et al. (2008), who have calculated the averaged photon escape fraction $f_{\rm esc}(\lambda)$ from observations of 10,000 nearby galaxies convolved with galactic dust models. We fit their results with four segments as

$$f_{\rm esc}(\lambda) = \begin{cases} 0.688 + 0.556\ \log\lambda\ ;\ \lambda \leq 0.165 \\ 0.151 - 0.136\ \log\lambda\ ;\ 0.165 < \lambda \leq 0.22 \\ 1.0 + 1.148\ \log\lambda\ ;\ 0.22 < \lambda \leq 0.422 \\ 0.728 + 0.422\ \log\lambda\ ;\ \lambda > 0.422\ , \end{cases} \tag{15}$$

with $\lambda$ in microns, and assume it to be universal or independent of redshift. The escape fraction $f_{\rm esc} \approx 0$ above $\approx 10$ eV as photons above this energy are absorbed by galactic gas. A feature of this model (Driver et al. 2008) is that the total amount of stellar energy absorbed by dust, in our local universe, is equivalent to the observed total luminosity density in infrared photons. The emission from luminous infrared galaxies, some of which may have an AGN core, is an added correction to the infrared EBL (see also Kneiske et al. 2004).

## 4. Results

We use Models A – E for the SFR+IMF combinations and equations (12) and (14), respectively, to calculate the EBL at $z = 0$ and luminosity density at $z = 0.1$ in starlight component, and compare with data. The results, with numerical integrations carried out by the multidimensional adaptive Monte Carlo code Vegas (Lepage 1978; 1980), are plotted in Figs. 4 and 5 for the SPL (left panels) and BPL (right panels) models of the $L - M$ relation.

To plot the luminosity density data points, in Fig. 4, we took the AB magnitude data $m_{AB} \equiv j + 2.5 \log h$ with $j = -2.5 \log(L_\epsilon/\text{W Hz}^{-1}\text{Mpc}^{-3}) + 34.1$ and converted them to luminosity density as $\epsilon L_\epsilon = h(c/\lambda)10^{13.64-m_{AB}/2.5}$ W Mpc$^{-3}$. The factor 34.1 comes from $2.5 \log(4.345 \times 10^{13})$, where $4.345 \times 10^{13}$ W Hz$^{-1}$ Mpc$^{-3}$ is the minimum of the absolute AB magnitude scale. Note that all data points are not measured at the same redshift or corrected to $z = 0$ as they come from different surveys: The Sloan Digital Sky Survey (*SDSS*), the Two Micron All Sky Survey (*2MASS*), the Two-Degree Field Galaxy Redshift Survey (*2dFGRS*) and the Galaxy Evolution Explorer (*GALEX*). The data points by Budavari et al. (2005) are calculated for redshift 0.07 – 0.13 and the mean redshift is 0.1 for the data points by Blanton et al. (2003). The data point by Norberg et al. (2002) and those by Cole et al. (2001) are corrected to $z = 0$. The redshift for Kochanek et al. (2001) data point is 0.03. Note that we plotted our luminosity density models A–E for redshift 0.1 to be consistent with most data points.

The three EBL data points in Fig. 5, in the UV band, are calculated by Bernstein, Freedman & Madore (2002) using measurements from the Hubble Space Telescope (*HST*). However, revised (Mattila 2003; Bernstein, Freedman & Madore 2005) and re-revised (Bernstein 2007) estimates have put substantial uncertainty on these data points. The rest of the data points come from analyzing measurements by the Diffuse Infrared Background Experiment (*DIRBE*) onboard the Cosmic Background Explorer (*COBE*) satellite by different authors (Dwek & Arendt 1998a; Gorjian, Wright & Chary 2000; Wright & Reese 2000; Cambrésy et al. 2001 and Levenson, Wright & Johnson 2007). This is the reason for multiple data points at the same energies. Note that the $\sim 1$ eV (1.25 $\mu$m) data point by Levenson, Wright & Johnson (2007) is really a $1\sigma$ limit. We plot only those upper limits (Dwek & Arendt 1998a; Hauser et al. 1998) and lower limits (Madau & Pozzetti 2000; Fazio et al. 2004) which are directly derived from the *DIRBE* and *HST* data.

Given a combination of mixed data points, Models A, B and D fare well reproducing the luminosity density data in Fig. 4 with the SPL model of $L - M$ relation (left panel) given by equation (4). These models miss the two data points at the smallest and largest (within $2\sigma$) wavelengths, however. In case of the BPL model of $L - M$ relation (right panel) given by equation (5), Models A, B and D agree with two small wavelength data points better

than the SPL model, but miss most data points at longer wavelengths. Models C and E are systematically lower than all data points for both the SPL and BPL cases. The integrated total energy output by stars, using Model B (SPL), is $1.2 \times 10^{35}$ W Mpc$^{-3}$ before dust absorption and $0.7 \times 10^{35}$ W Mpc$^{-3}$ after dust absorption. As for comparison, Driver et al. (2008) calculated these values as $1.6 \times 10^{35}$ W Mpc$^{-3}$ and $0.9 \times 10^{35}$ W Mpc$^{-3}$, respectively.

Comparing with EBL data in Fig. 5, we find again that Models A, B and D with the SPL $L - M$ relation (left panel) represent the data points better than all other models in both SPL and BPL cases. Models A, B and D in the BPL case are consitently lower, below 2 eV, than the SPL case, a reflection of the trend observed in the luminosity density plots as well. Models C and E in both the SPL and BPL cases (right panel) are below the *HST* lower limits (Madau & Pozzetti 2000). None of our models are able to reproduce EBL data below 1 eV hinting that an extra component is required for modeling infrared data.

Models A, B and D involve Salpeter A IMF which predicts more stars forming below $\sim 2M_{\odot}$ than the Baldry & Glazebrook (2003) IMF used in Models C and E. This may be one reason why these models underproduce the local luminsoity density and EBL, since stars with $\lesssim 2M_{\odot}$ dominantly produce $\lesssim 2$ eV photons. The other affecting factors are the differences in SFR models (see Fig. 3) and mass-to-light ratio. With $f_L > 1$ in equation (5), for the Baldry-Glazebrook IMF, it may be possible to close gaps between Models C and E with other models with BPL $L - M$ relation. However, we do not explore that possibility in the present paper. For the purposes of $\gamma$-ray astronomy, any of the Models A, B or D can reproduce local UV/optical EBL data. Next we compare our EBL models to the models by other authors.

### 4.1. Comparisons with other authors

Among several existing models of the EBL, the one by Primack, Bullock & Somerville (2005), plotted in Fig. 6 is used to be considered as the "Low" EBL model. It is consistent with the lower limits from the galaxy counts above $\sim$0.5 eV. An updated version of the fast evolution model by Stecker, Malkan & Scully (2006) is also plotted in Fig. 6. This is considered to be the "High" EBL model. The best-fit model by Kneiske et al. (2004), plotted here, and the phenomenological fits by Dermer (2007), not plotted here, are generally in between these two models.

Primack, Bullock & Somerville (2005) used Monte Carlo simulations of galaxy evolution and emission by the evolving galaxy population to calculate their EBL model. Kneiske, Mannheim & Hartmann (2002); and Kneiske et al. (2004) used the outcome of the simu-

lations of stellar population luminosity at different redshift, and integrated over redshift to calculate the EBL. Stecker, Malkan & Scully (2006) assumed that the observed luminosity of a galaxy at 60 $\mu m$ can be used to calculate its luminosity at all wavelengths, and used galaxy luminosity functions to calculate the EBL. In our models, we used blackbody emission from stars, based on the solar models, and convolve with the star formation and initial mass function models to calculate the EBL. These methods, therefore, are not directly comparable to each other. However, assumptions about an SFR or/and an IMF model(s) should affect all methods as also shown by Kneiske, Mannheim & Hartmann (2002); Kneiske et al. (2004). Indeed the variations between our EBL models A–E results from the differences in SFR and IMF combinations.

Our models (A, SPL), (B, SPL) and (D, SPL) are consistent with the *HST* lower limits above ∼1 eV and agree with the EBL model by Primack, Bullock & Somerville (2005) in the ∼1–3 eV range. At energies lower than ∼1 eV our models are lower than all other models. This is probably because the infrared EBL component, from dust radiation; luminous infrared galaxies and post main-sequence stars, becomes important at these lower energies. At energies above ∼3 eV all other EBL models are higher than our models. There may be additional contributions from AGN and white dwarfs at these higher energies, however due to a lack of data points comparisons between the models above ∼3 eV become less meaningful.

Both the models (B, SPL) and (D, SPL) better represent the luminosity density data in Fig. 4 than the model (A, SPL) and can be used as our best-fit EBL models. For illustration and further calculations, we have chosen to use Model B, SPL plotted in Fig. 6. We have also plotted our Model (B, BPL) for comparisions.

### 4.2. Evolution with redshift

Understanding the evolution of the background light with redshift is a key to $\gamma$-ray astronomy, which we discuss in the next section. The mean-free-path for $\gamma\gamma$ absorption with the EBL spans astronomical distances, over which the EBL itself changes noticeably. We have plotted the comoving EBL energy density at different redshifts 0–5 in Fig. 7 using equation (13) for the Model B, SPL. Initially the EBL density increases with redshift because of the sharp rise in star formation (see Fig. 3) below $z \sim 2$ and a decreasing volume. At redshift $\gtrsim 2$, the EBL density decreases because the total number of stars formed up to that redshift from $z = 6$ decreases. The contribution to the EBL above ∼2–3 eV dominantly comes from high mass stars. Since the livetimes of high-mass stars are shorter, their contribution to the EBL at a particular $z$ is mostly determined by how many of them are formed at $\sim z$ (see Fig. 1). On the other hand the overall population of low mass stars, which dominantly

produce lower energy photons, increases with decreasing redshift. As a result, the ratio of high-energy photon density increases with redshift (as evidenced by the hump at ∼7 eV) compared to the low energy photon density reflecting a decreasing overall population of low mass stars for $z \to 6$.

## 5. Implications for $\gamma$-ray Astronomy

High-energy photons in the ∼10–300 GeV energy range from sources such as GRB at $z \gtrsim 0.5$ are subject to $\gamma\gamma \to e^+e^-$ absorption by the EBL starlight photons as we modeled here. To calculate the $\gamma\gamma$ absorption opacity one needs to take into account an evolving EBL with redshift as plotted in Fig. 7. We calculate this opacity both numerically, using interpolation to the exact results from Model B, SPL calculation, and analytically, by fitting the Model B, SPL results.

We provide such a fit below and plot it in Fig. 8 at different redshift overlaid with numerical calculation. The polynomial fit parameters are

$$\begin{aligned}
\log(\epsilon_1 u_{\epsilon_1}/\text{ergs cm}^{-3}) &= A_0 + A_1 x + A_2 x^2 + A_3 x^3 + A_4 x^4 \\
x &= \log(\epsilon_1\ (\text{eV})/(1+z_1)) \\
A_0 &= -14.4829 + 0.8275 z_1 - 0.2451 z_1^2 + 0.0046 z_1^3 + 0.0043 z_1^4 - 0.0004 z_1^5 \\
A_1 &= 0.3157 - 1.105 z_1 + 1.1026 z_1^2 - 0.4764 z_1^3 + 0.09 z_1^4 - 0.0062 z_1^5 \\
A_2 &= \begin{cases} -1.9888 + 1.6527 z_1 + 1.0294 z_1^2\ ;\ z_1 < 0.8 \\ -0.5549 - 0.0295 z_1 - 0.1133 z_1^2 + 0.0079 z_1^3\ ;\ z_1 > 0.8 \end{cases} \\
A_3 &= -0.1507 + 0.9114 z_1 - 1.8907 z_1^2 + 0.8816 z_1^3 - 0.1837 z_1^4 + 0.0141 z_1^5 \\
A_4 &= 0.3014 - 3.5371 z_1 + 2.4574 z_1^2 - 0.8474 z_1^3 + 0.1343 z_1^4 - 0.0079 z_1^5\ , \qquad (16)
\end{aligned}$$

where $\epsilon_1 = \epsilon(1+z_1)$. The fit is generally good at the tens of percentage level of the numerical results for $\epsilon_1 \gtrsim 0.5$ eV for all redshift $z_1 \leq 5$.

With a fit to the diffuse background photons, in equation (16), we can easily calculate the optical depth of $\gamma\gamma$ absorption for an energetic photon originating at redshift $z$ with observed energy $E$ as (Gould & Schréder 1967; Brown, Mikaelian & Gould 1973)

$$\begin{aligned}
\tau_{\gamma\gamma}(E,z) &= c\int_0^z dz_1 \left|\frac{dt}{dz_1}\right| \\
&\quad \times \int_0^\infty d\epsilon_1 \int_{-1}^1 d\cos\theta \frac{1}{2}\frac{u_{\epsilon_1}}{\epsilon_1}(1-\cos\theta)\sigma_{\gamma\gamma}(s) \\
&= c\pi r_e^2 \frac{m_e^4 c^8}{E^2}\int_0^z \frac{dz_1}{(1+z_1)^2}\left|\frac{dt}{dz_1}\right|
\end{aligned}$$

$$\times \int_{m_e^2c^4/E(1+z_1)}^{\infty} d\epsilon_1 \frac{u_{\epsilon_1}}{\epsilon_1} \bar{\varphi}[s_0(\epsilon_1)]. \quad (17)$$

for an isotropic background photon field. Here $\sigma_{\gamma\gamma}(s)$ is the total $\gamma\gamma \rightarrow e^+e^-$ cross-section (see, e.g., Jauch & Rohrlich 1955) and $s = E(1+z_1)\epsilon_1(1-\cos\theta)/2m_e^2c^4$ is the center-of-mass energy squared. The function $\bar{\varphi}[s_0]$, with $s_0 = E(1+z_1)\epsilon_1/m_e^2c^4$, is given in Gould & Schréder (1967). The threshold energy for $e^+e^-$ pair production from the condition $s_0 = 1$ is $\epsilon_{1,\rm th} \approx m_e^2c^4/E(1+z_1)$. The lower limit of the energy integration $\epsilon_{1,\rm th} \approx 1$ eV and $\sim 250/(1+z_1)$ GeV $\gamma$-rays interact dominantly with these photons. Higher energy $\gamma$-rays mainly interact with softer photons, at an energy range where the re-processed dust emission dominates the EBL and our models do not fit the data. With an upper limit $\epsilon_{1,\rm max} \approx 10$ eV, it is safe to use equation (17) in the ∼10–300 GeV $\gamma$-ray energy range for redshift $\gtrsim 0.5$. Note that this the relevant energy range for the Large Area Telescope on board the *Fermi Gamma Ray Space Telescope*. Air Cherenkov Telescopes also become sensitive to $\gamma$-rays $\gtrsim$50 GeV. The survival probability for a $\gamma$-ray created at redshift $z$ to reach Earth is $\exp[-\tau_{\gamma\gamma}(E,z)]$. The observed flux of $\gamma$-rays is attenuated by this factor from the source flux.

We have plotted the $\gamma\gamma$ opacity ($\tau_{\gamma\gamma}$) in Fig. 9 for redshift 0.5–5.0 and observed $\gamma$-ray energy 10–300 GeV using equation (17). The solid and dashed lines correspond to the exact calculation and calculation using the fit in equation (16) respectively. As can be seen, the two methods of calculation give results within tens of percent. For $z \geq 3$ (right panel) we have divided $\tau_{\gamma\gamma}$ with constant factors given on the plot to avoid cluttering of different curves. We also provide our exact calculation of $\tau_{\gamma\gamma}$ in Table 1 for different redshift and $\gamma$-ray energies. The relation $\tau_{\gamma\gamma} = 1$ (Fig. 10), sometimes referred to as the Fazio-Stecker relation (Fazio & Stecker 1970), corresponds to a $\gamma$-ray horizon of the universe.

With the calculated opacities, we can calculate the true $\gamma$-ray flux of a distant source before absorption in the EBL by multiplying the observed flux $f_E$ with the factor $\exp[\tau_{\gamma\gamma}(E)]$. In case of the furthest known blazar 3C279 at $z = 0.536$, the flux data points measured by MAGIC (Albert et al. 2008) are plotted in Fig. 11. We have also plotted the deabsorbed data points (open circles) using our EBL Model B (SPL) and a power-law fit $dN/dE = N_0(E/200\ \text{GeV})^{-\Gamma}$ with $N_0 = 1.5 \times 10^{-9}$ TeV$^{-1}$ cm$^{-2}$ s$^{-1}$ and $\Gamma = 2.8$. The deabsorbed spectrum of 3C 279 thus becomes harder than the observed value of $\Gamma = 4.11$ (Albert et al. 2008). Note, however, that our $\gamma\gamma$ opacity calculation is less reliable for the highest energy data point at 474 GeV. The $\Gamma$ for the deabsorbed spectrum, thus, can be $\lesssim 2.78$ if $\tau_{\gamma\gamma}$ is much larger than our estimate.

Simple Fermi mechanisms of particle acceleration in both relativitic and non-relativistic shocks, result in particle spectra $dN/dE \propto E^{-p}$ with $p \approx 2$. In the case of a one-zone synchro-Compton mechanism to produce TeV $\gamma$-rays at the shocks, the source spectrum of

$\gamma$-rays typically should be larger than $\Gamma = (p+1)/2 \approx 1.5$. Spectra harder than the simple-minded limiting value may arise in a number of scenarios. For a special environment at or surrounding the shocks, effects such as a cutoff of shock-accelerated elecron spectrum below a very high energy $\sim$GeV (Katarzyński et al. 2006; Stern & Poutanen 2008) or internal $\gamma\gamma$ absorption in a dense region of quasi mono-energetic soft photons (Aharonian, Khangulyan & Costamante 2008) may result in a very hard spectrum $\Gamma < 1.5$ over a short energy range. Acceleration at shear flows (Stawarz & Ostrowski 2002; Rieger & Duffy 2006) or Monte Carlo shock-acceleration models may also result in $\Gamma < 1.5$ (Virtanen & Vainio 2005; Stecker et al. 2007).

Models with multiple spectral components, arising from multiple zones, are attractive to explain observed hard blazar spectra. Recently Böttcher, Dermer & Finke (2008) have invoked such a model of Compton upscattering of CMB photons in large scale jet to explain hard spectrum of 1ES 1101-232. Also, cosmic-ray acceleration and interactions at the shocks and subsequent cascade in the EBL-CMB may also produce very hard $\gamma$-ray spectra (Coppi & Aharonian 1997). However, such models cannot explain highly variable TeV spectra, e.g., from 3C 279 (Albert et al. 2008).

## 6. Conclusions

We have derived a class of well-defined models for the spectral energy density of the EBL. The models with modified Salpeter A initial mass function, a single power-law mass-luminosity relation and Cole et al. (2001) or Hopkins & Beacom (2006) star formation history reasonably fit the EBL UV-optical data and the luminosity density in our local universe.

Our models are based on the underlying assumption that the bulk of the EBL radiation between $\sim 0.1 - 10$ eV is due to stellar radiations absorbed by dust, which can be determined from recent analyses of galaxies by Driver et al. (2008). This approach differs from models by Stecker, Malkan & Scully (2006) based on luminosity evolution of galactic spectral energy distributions, which is limited to the accuracy of the available observational data used in the survey. Without need of a population synthesis code (e.g., models by Primack, Bullock & Somerville 2005) or fits to the results of such a code (e.g., models by Kneiske, Mannheim & Hartmann 2002), our model is based on well-studied results from stellar astronomy.

The sources of uncertainties in our models are the (i) main-sequence age of the star and stellar luminosity, discussed earlier, (ii) star formation history and initial mass function, and (iii) dust absorption. We have already discussed point (ii) in some details using five SFR+IMF models. Note that in all those models, the IMF was assumed to be independent

of redshift. In principle the normalization of the IMF or even its shape may depend on $z$. Nevertheless, a universal IMF fits SFR data reasonably well. The evolution of the dust absorption model with redshift, which we have not taken into account, is of potentially greater concern. At high redshift it is more reasonable to assume that the dust absorption (escape) fraction would be higher (lower), so that the stellar contribution to the EBL at high $z$ would be less than if using a constant absorption fraction. A more detailed examination of these issues are under further study (Finke et al., in perperation).

We have provided an analytic fit to our best-fit EBL model and its evolution with redshift. This result can be used to calculate, as we have done in this work, opacity of the universe to ∼10–300 GeV $\gamma$-rays relevant for the high energy data from the *Fermi Gamma Ray Space Telescope* and Air Cherenkov Telescopes, and estimating unknown quantities such as the spectrum and energy at production of the distant GRBs and blazars such as 3C 279.

We thank Eli Dwek, Claude-André Faucher-Giguère, Dieter Hartmann, Tanja Kneiske, Kalevi Mattila and Floyd Stecker for helpful comments. The work of S.R. and J.D.F. was supported by the National Research Council Research associateship program at the Naval Research Laboratory. The work of C.D.D. was supported by the Office of Naval Research.

## REFERENCES

Aharonian, F.A., et al. 2005, A&A, 442, 895

Aharonian, F.A., et al. 2006a, A&A, 455, 461

Aharonian, F.A., et al. 2006b, Nature, 440, 1018

Aharonian, F.A., et al. 2007, A&A, 473, L25

Aharonian, F.A., Khangulyan, D. & Costamante, L. 2008, MNRAS, 387, 1206

Albert, J., et al. 2006, ApJ, 642, L119

Albert, J., et al. 2007, ApJ, 667, L21

Albert, J., et al. 2008, Science, 320, 1752

Baldry, I.K. & Glazebrook, K. 2003, ApJ, 593, 258

Bernstein, R.A., Freedman, W.L. & Madore, B.F. 2002, ApJ, 571, 56

Bernstein, R.A., Freedman, W.L. & Madore, B.F. 2005, ApJ, 632, 713

Bernstein, R.A. 2007, ApJ, 666, 663

Binney, J. & Merrifield, M. 1998, Galactic Astronomy (Princeton)

Blanton, M.R., et al. 2003, ApJ, 592, 819

Böttcher, M., Dermer, C.D. & Finke, J.D. 2008, ApJ, 679, L9

Bressan, A., Fagotto, F., Bertelli, G. & Chiosi, C. 1993, A&AS, 100, 647

Brown, R.W., Mikaelian, K.O. & Gould, R.J. 1973, Astrophysical Letters, 14, 203

Budavari, T., et al. 2005, ApJ, 619, L31

Cambrésy, L., Reach, W.T., Beichman, C.A. & Jarrett, T.H. 2001, ApJ, 555, 563

Cole, S., et al. 2001, MNRAS, 326, 255

Coppi, P. S., & Aharonian, F. A. 1997, ApJ, 487, L9

Dermer, C.D. 2007, arXiv:0711.2804 [astro-ph], in 30th ICRC, Mérida, Mexico.

Driver, S.P., et al. 2008, arXiv:0803.4164 [astro-ph]

Dwek, E. & Arendt, R.G. 1998, ApJ, 508, L9

Dwek, E., et al. 1998, ApJ, 508, 106

Faucher-Giguère, C.-A., Lidz, A., Hernquist, L., & Zaldarriaga, M. 2008, ApJ, 682, L9

Fazio, G.G. & Stecker, F.W. 1970, Nature, 226, 135

Fazio, G.G., et al. 2004, ApJS, 154, 39

Finke, J.D., et al., in preperation

Fukugita, M. & Peebles, P.J.E. 2004, ApJ, 616, 643

Gorjian, V., Wright, E.L. & Chary, R.R. 2000, ApJ536, 550

Gould, R.J. & Shréder, G. 1966, Phys. Rev. Lett. 16, 252

Hauser, M.G., et al. 1998, ApJ, 508, 25

Hopkins, A.M. & Beacom, J.F. 2006, ApJ, 651, 142

Inoue, Y., Totani, T. & Ueda, Y. 2008, ApJ, 672, L5

Jauch, J.M. & Rohrlich, F. 1955, The Theory of Photons and Electrons (Cambridge: Addison-Wesley)

Katarzyński, K., Ghisellini, G., Tavecchio, F., Gracia, J. & Maraschi, L. 2006, MNRAS, 368, L52

Kneiske, T.M., Mannheim, K. & Hartmann, D.H. 2002, A&A 386, 1

Kneiske, T.M., Bretz, T., Mannheim, K. & Hartmann, D.H. 2004, A&A 413, 807

Kochanek, C.S., et al. 2001, ApJ, 560, 566

Lepage, G.P. 1978, Journal of Computational Physics, 27, 192

Lepage, G.P. 1980, "VEGAS: An Adaptive Multidimensional Integration Program," Publication CLNS-80/447, Cornell University

Levenson, L.R., Wright, E.L. & Johnson 2007, ApJ, 666, 34

Madau, P., et al. 1996, MNRAS, 283, 1388

Madau, P. & Pozzetti, L. 2000, MNRAS, 312, L9

Malkan, M.A. & Stecker, F.W. 1998, ApJ, 496, 13

Malkan, M.A. & Stecker, F.W. 2001, ApJ, 555, 641

Mattila, K. 2003, ApJ, 591, 119

Mazin, D. & Raue, M. 2007, A&A 471, 439

Mushotzky, R.F., Cowie, L.L., Barger, A.J. & Arnaud, K.A. 2000, Nature, 404, 459

Nishikov, A.I. 1961, Zh. Experimen. i Theo. Fiz. 41, 549

Norberg, P., et al. 2002, MNRAS, 336, 907

Persic, M., & de Angelis, A. 2008, A&A, 483, 1

Primack, J.R., Bullock, J.S., Somerville & MacMinn, D. 1999, APh, 11, 93

Primack, J.R., Bullock, J.S. & Somerville, R.S. 2005, in High Energy Gamma-Ray Astronomy, ed. F.A. Aharonian, H. Volk, & D. Horns (Melville: AIP), 23

Reimer, A. 2007, ApJ, 665, 1023

Rieger, F.M. & Duffy, P. 2006, ApJ, 652, 1044

Ruiz-Lapuente, P., Cassé, M. & Vangioni-Flam, E. 2001, ApJ, 549, 483

Salamon, M. H., & Stecker, F. W. 1998, ApJ, 493, 547

Salpeter, E.E. 1955, ApJ, 121,161

Schmidt-Kaler, Th. 1982, in Landolt-Bornstein: Numerical data and Functional Relationships in Science and Technology, vol. 2b, ed. K. Schaifers & H.H. Voigt (Springer:Berlin)

Stanev, T. & Franceschini, A. 1998, ApJ, 494, L159

Stawarz, L. & Ostrowski, M. 2002, ApJ, 578, 763

Stecker, F.W., de Jager, O.C. 1993, ApJ, 415, L71

Stecker, F.W., Malkan, M.A. & Scully, S.T. 2006, ApJ, 648, 774

Stecker, F.W., Baring, M.G. & Summerlin, E.J. 2007, ApJ, 667, L29

Stern, B.E. & Poutanen, J. 2008, MNRAS, 383, 1695

Strigari, L.E., Beacom, J.F., Walker, T.P. & Zhang, P. 2005, JCAP, 04, 017

Virtanen, J.J.P. & Vainio, R. 2005, ApJ, 621, 313

Watanabe, K., Hartmann, D.H., Leising, M.D. & The, L.-S. 1999, ApJ, 516, 285

Wright, E.L. & Reese, E.D. 2000, ApJ, 545, 43

Table 1. $\gamma$ ray absorption opacity ($\tau_{\gamma\gamma}$) with EBL Model B, SPL at different redshift

| $E_\gamma$ GeV | $z$ 0.5 | $z$ 1.0 | $z$ 1.5 | $z$ 2.0 | $z$ 2.5 | $z$ 3.0 | $z$ 3.5 | $z$ 4.0 | $z$ 4.5 | $z$ 5.0 |
|---|---|---|---|---|---|---|---|---|---|---|
| 13.18 | 0.0000 | 0.0004 | 0.0025 | 0.0081 | 0.0174 | 0.0284 | 0.0387 | 0.0468 | 0.0526 | 0.0563 |
| 14.45 | 0.0000 | 0.0007 | 0.0041 | 0.0123 | 0.0253 | 0.0400 | 0.0533 | 0.0635 | 0.0708 | 0.0752 |
| 15.85 | 0.0001 | 0.0013 | 0.0065 | 0.0183 | 0.0359 | 0.0551 | 0.0721 | 0.0849 | 0.0938 | 0.0993 |
| 17.38 | 0.0002 | 0.0021 | 0.0099 | 0.0264 | 0.0498 | 0.0747 | 0.0961 | 0.1121 | 0.1229 | 0.1294 |
| 19.05 | 0.0003 | 0.0034 | 0.0146 | 0.0372 | 0.0680 | 0.0998 | 0.1266 | 0.1462 | 0.1594 | 0.1670 |
| 20.89 | 0.0005 | 0.0053 | 0.0212 | 0.0515 | 0.0914 | 0.1316 | 0.1649 | 0.1889 | 0.2046 | 0.2136 |
| 22.91 | 0.0008 | 0.0079 | 0.0300 | 0.0700 | 0.1213 | 0.1718 | 0.2127 | 0.2418 | 0.2604 | 0.2708 |
| 25.12 | 0.0014 | 0.0116 | 0.0416 | 0.0940 | 0.1592 | 0.2221 | 0.2722 | 0.3068 | 0.3286 | 0.3405 |
| 27.54 | 0.0021 | 0.0167 | 0.0568 | 0.1246 | 0.2070 | 0.2849 | 0.3452 | 0.3861 | 0.4113 | 0.4249 |
| 30.20 | 0.0032 | 0.0234 | 0.0765 | 0.1636 | 0.2671 | 0.3622 | 0.4342 | 0.4818 | 0.5108 | 0.5258 |
| 33.11 | 0.0047 | 0.0323 | 0.1019 | 0.2131 | 0.3417 | 0.4566 | 0.5415 | 0.5965 | 0.6292 | 0.6457 |
| 36.31 | 0.0068 | 0.0440 | 0.1345 | 0.2755 | 0.4335 | 0.5709 | 0.6698 | 0.7324 | 0.7687 | 0.7869 |
| 39.81 | 0.0096 | 0.0592 | 0.1763 | 0.3533 | 0.5454 | 0.7078 | 0.8215 | 0.8916 | 0.9317 | 0.9515 |
| 43.65 | 0.0134 | 0.0789 | 0.2295 | 0.4493 | 0.6804 | 0.8696 | 0.9984 | 1.0763 | 1.1203 | 1.1410 |
| 47.86 | 0.0183 | 0.1045 | 0.2963 | 0.5667 | 0.8410 | 1.0582 | 1.2027 | 1.2883 | 1.3357 | 1.3580 |
| 52.48 | 0.0248 | 0.1375 | 0.3797 | 0.7085 | 1.0296 | 1.2761 | 1.4361 | 1.5293 | 1.5798 | 1.6037 |
| 57.54 | 0.0334 | 0.1798 | 0.4828 | 0.8773 | 1.2479 | 1.5247 | 1.7004 | 1.8002 | 1.8545 | 1.8788 |
| 63.10 | 0.0446 | 0.2335 | 0.6084 | 1.0751 | 1.4978 | 1.8049 | 1.9955 | 2.1019 | 2.1592 | 2.1844 |
| 69.18 | 0.0593 | 0.3010 | 0.7590 | 1.3034 | 1.7795 | 2.1166 | 2.3210 | 2.4340 | 2.4933 | 2.5199 |
| 75.86 | 0.0785 | 0.3848 | 0.9365 | 1.5636 | 2.0939 | 2.4597 | 2.6772 | 2.7958 | 2.8578 | 2.8840 |
| 83.18 | 0.1033 | 0.4871 | 1.1428 | 1.8562 | 2.4409 | 2.8337 | 3.0635 | 3.1867 | 3.2510 | 3.2783 |
| 91.20 | 0.1349 | 0.6102 | 1.3792 | 2.1814 | 2.8190 | 3.2373 | 3.4784 | 3.6056 | 3.6714 | 3.6997 |
| 100.00 | 0.1750 | 0.7558 | 1.6461 | 2.5388 | 3.2267 | 3.6688 | 3.9199 | 4.0500 | 4.1189 | 4.1456 |
| 109.65 | 0.2250 | 0.9258 | 1.9440 | 2.9260 | 3.6617 | 4.1259 | 4.3848 | 4.5181 | 4.5881 | 4.6164 |
| 120.23 | 0.2862 | 1.1201 | 2.2714 | 3.3401 | 4.1212 | 4.6048 | 4.8703 | 5.0067 | 5.0768 | 5.1051 |
| 131.83 | 0.3596 | 1.3394 | 2.6262 | 3.7782 | 4.6013 | 5.1010 | 5.3727 | 5.5094 | 5.5818 | 5.6089 |
| 144.54 | 0.4466 | 1.5839 | 3.0055 | 4.2369 | 5.0978 | 5.6109 | 5.8874 | 6.0243 | 6.0973 | 6.1244 |
| 158.49 | 0.5473 | 1.8526 | 3.4069 | 4.7131 | 5.6059 | 6.1303 | 6.4087 | 6.5471 | 6.6193 | 6.6479 |
| 173.78 | 0.6626 | 2.1416 | 3.8259 | 5.1994 | 6.1200 | 6.6530 | 6.9323 | 7.0694 | 7.1430 | 7.1695 |
| 190.55 | 0.7923 | 2.4489 | 4.2581 | 5.6910 | 6.6349 | 7.1731 | 7.4531 | 7.5872 | 7.6624 | 7.6876 |

Table 1—Continued

| $E_\gamma$ GeV | $z$ 0.5 | $z$ 1.0 | $z$ 1.5 | $z$ 2.0 | $z$ 2.5 | $z$ 3.0 | $z$ 3.5 | $z$ 4.0 | $z$ 4.5 | $z$ 5.0 |
|---|---|---|---|---|---|---|---|---|---|---|
| 208.93 | 0.9363 | 2.7721 | 4.6986 | 6.1836 | 7.1457 | 7.6864 | 7.9641 | 8.0971 | 8.1708 | 8.1969 |
| 229.09 | 1.0925 | 3.1074 | 5.1405 | 6.6710 | 7.6465 | 8.1867 | 8.4607 | 8.5922 | 8.6658 | 8.6900 |
| 251.19 | 1.2597 | 3.4505 | 5.5803 | 7.1482 | 8.1314 | 8.6679 | 8.9390 | 9.0668 | 9.1404 | 9.1650 |
| 275.42 | 1.4362 | 3.7960 | 6.0133 | 7.6094 | 8.5944 | 9.1251 | 9.3916 | 9.5161 | 9.5892 | 9.6121 |
| 301.99 | 1.6204 | 4.1397 | 6.4326 | 8.0473 | 9.0297 | 9.5530 | 9.8138 | 9.9358 | 10.007 | 10.031 |

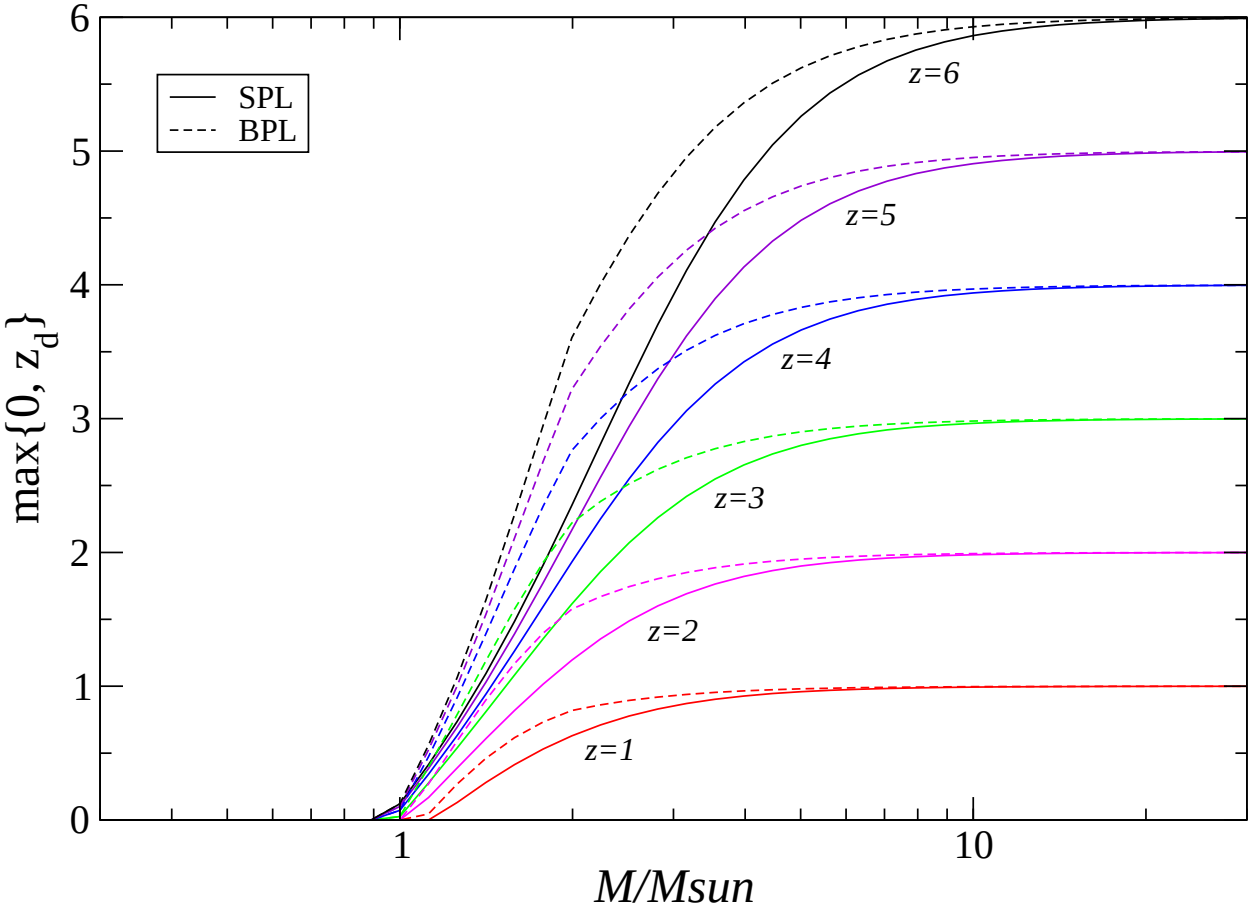


Fig. 1.— Plot of the redshift ($\max\{0,\ z_{\rm d}(M,z)\}$) at which a star of mass $M$ which was born at redshift $z$ =1 – 6 evolves off the main sequence using equation (10) and assuming the standard (0.7, 0.3, 0.7) ΛCDM cosmology. The two sets of curves correspond to SPL (dashed) and BPL (dotted) $L-M$ relation, respectively, in equations (4) and (5).

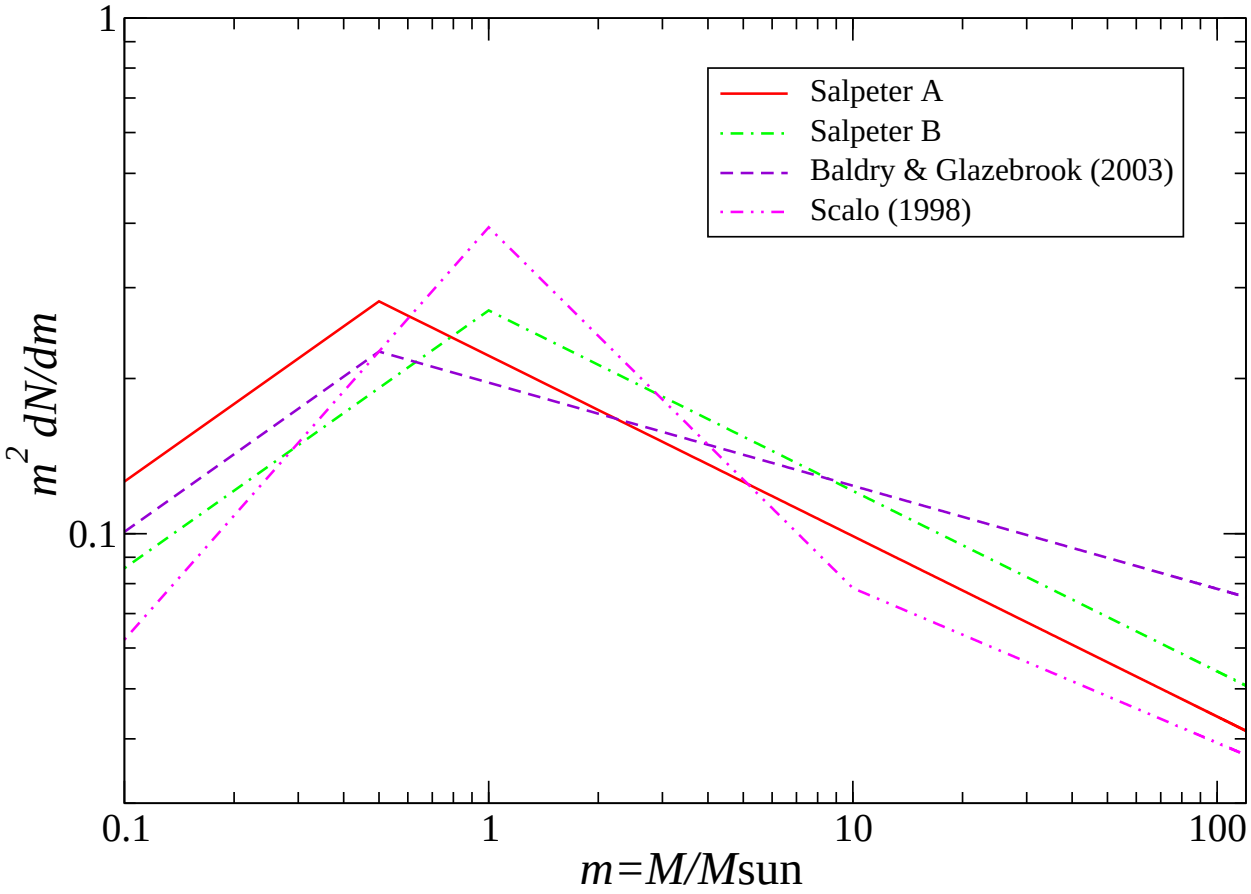


Fig. 2.— Initial mass function (IMF) models, assumed to be universal. The integral of $dN/d\ln M$ is set to unity over $M$=(0.1–120)$M_\odot$ range.

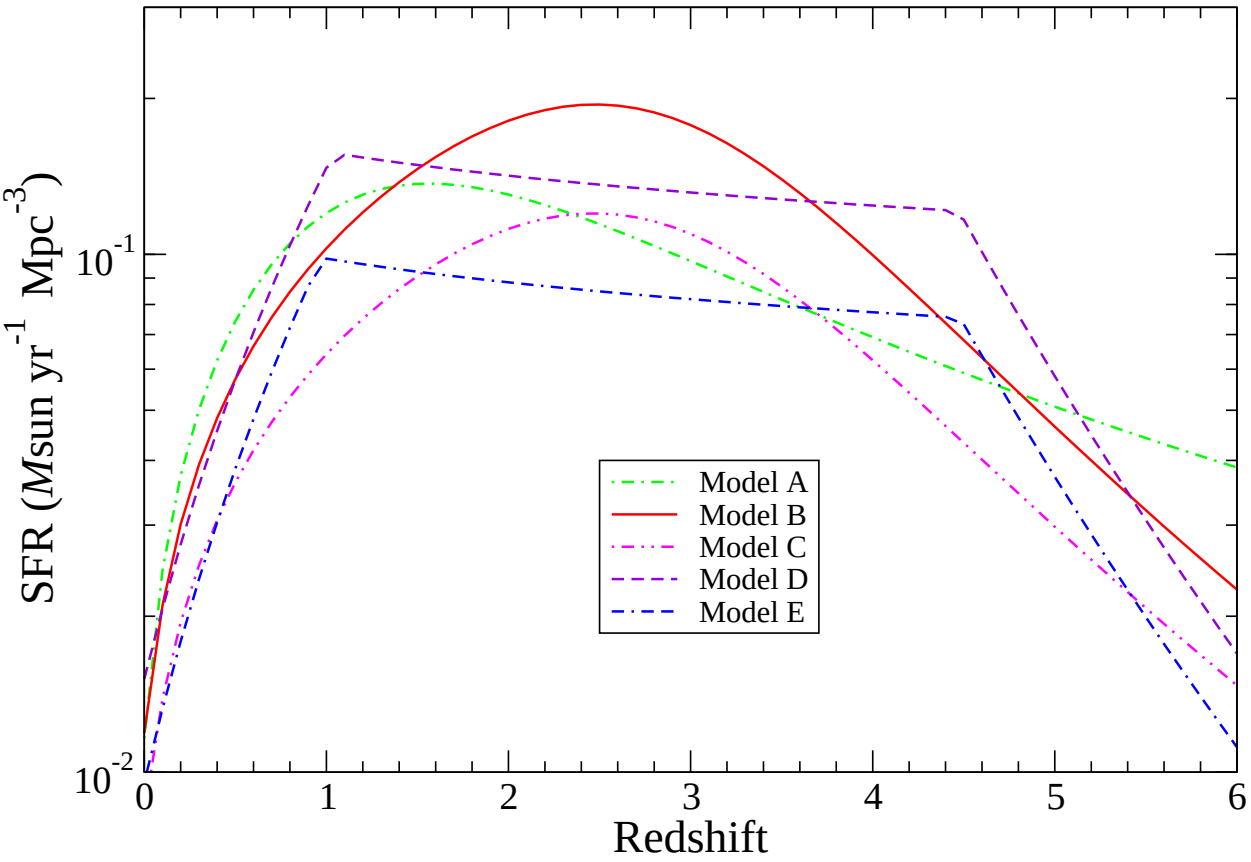


Fig. 3.— Models of SFR combined with specific IMF. *Model A* correspond to Cole et al. (2001) SFR with *Salpeter A* IMF, *Model B* correspond to Cole et al. (2001) SFR formula fitted by Hopkins & Beacom (2006) with *Salpeter A* IMF, *Model C* correspond to Cole et al. (2001) SFR formula fitted by Hopkins & Beacom (2006) with *Baldry-Glazebrook* IMF, *Model D* correspond to Hopkins & Beacom (2006) SFR with *Salpeter A* IMF and *Model E* correspond to Hopkins & Beacom (2006) SFR with *Salpeter A* IMF.

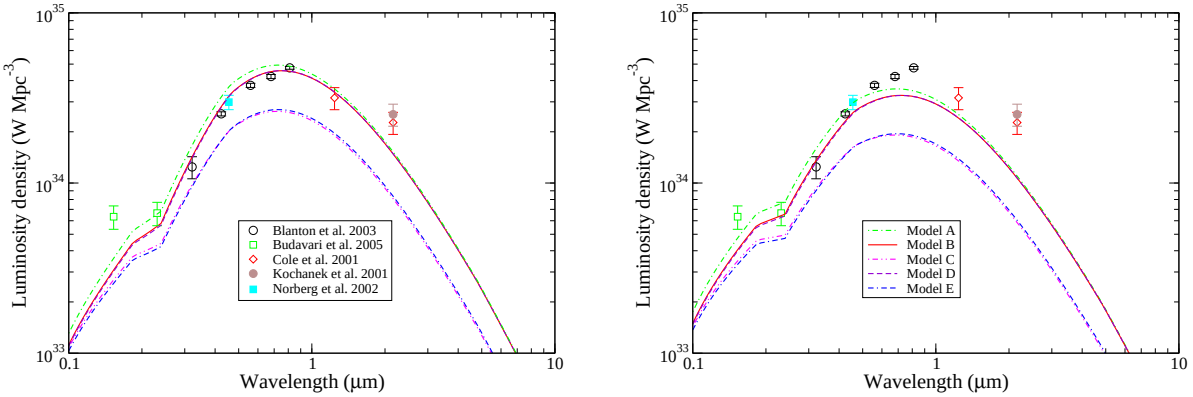


Fig. 4.— Total energy output or luminosity density, $\epsilon_1 L_{\epsilon_1}$ from equation (14), in direct starlight by our local ($z_1 = 0.1$) universe. The data points are from *SDSS*, *2MASS*, *2dFGRS* and *GALEX* surveys of local galaxies. The smooth lines are our calculations using equation (14) and based on SFR+IMF models A–E described in Section 3. The left and right panels correspond to the SPL and BPL models of $L - M$ relation, respectively, given by equations (4) and (5).

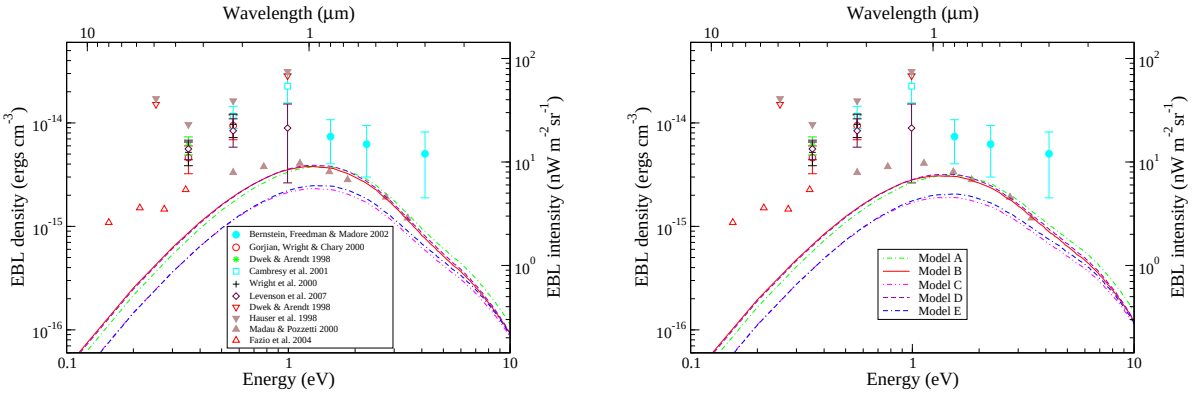


Fig. 5.— EBL energy density, $\epsilon u_\epsilon = \epsilon^2 dN(\epsilon, z = 0)/d\epsilon dV$ from equation (12), from direct starlight in our local universe. The smooth lines are calculated using equation (12) and correspond to SFR+IMF models A–E as defined in Section 3. The data points with errorbars, and lower (triangles) and upper (inverted triangles) limits are described in Sec. 4. *Left panel*— models with $L - M$ relation (SPL) in equation (4). *Right panel*— models with $L - M$ relation (BPL) in equation (5).

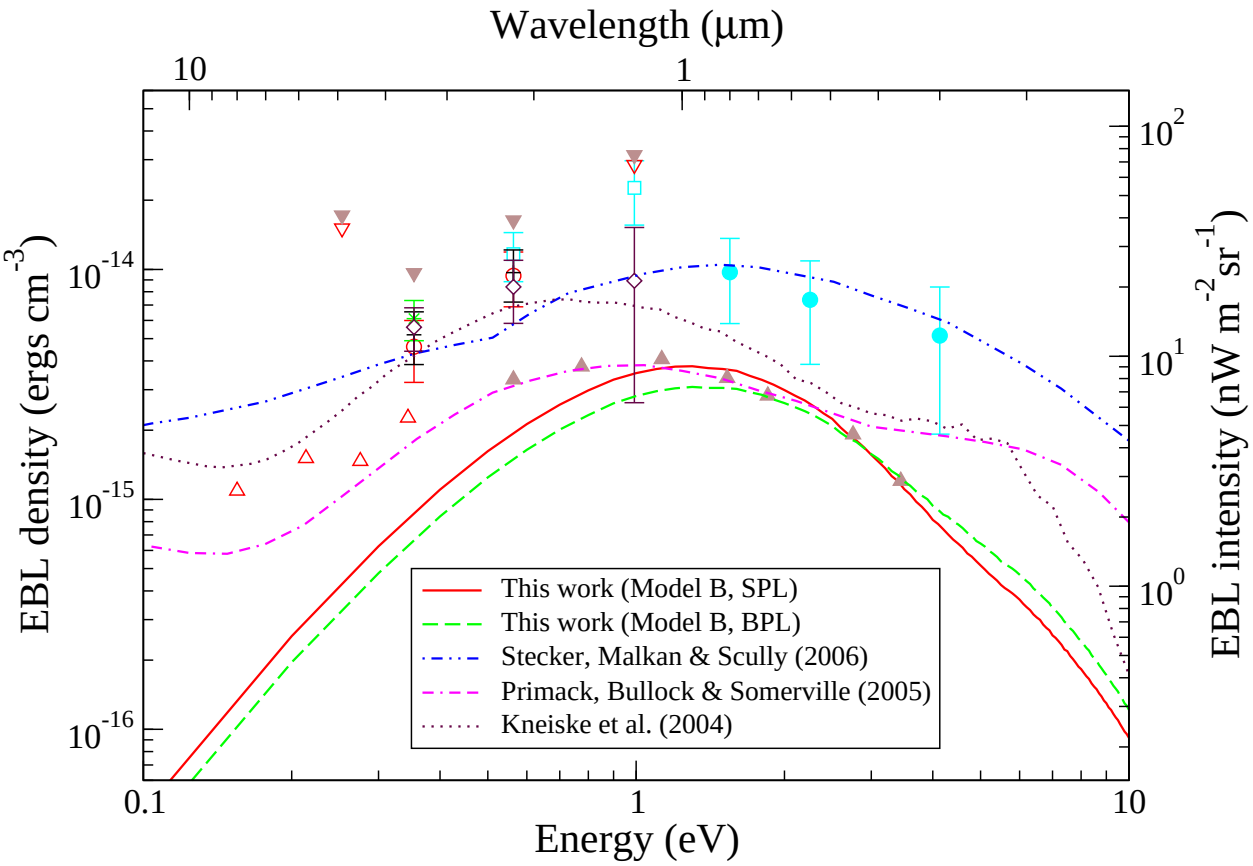


Fig. 6.— A comparison of the EBL models (B, SPL) and (B, BPL) derived in this paper with models by other authors. The updated fast evolution model by Stecker, Malkan & Scully (2006) is based on backward-evolution models of local galaxies. The models by Primack, Bullock & Somerville (2005) is based on Monte Carlo simulatons of galaxy evolution with initial conditions. The model by Kneiske et al. (2004) is based on results of population synthesis models. Our models are based on initial mass function and star formation models convolved with stellar properties.

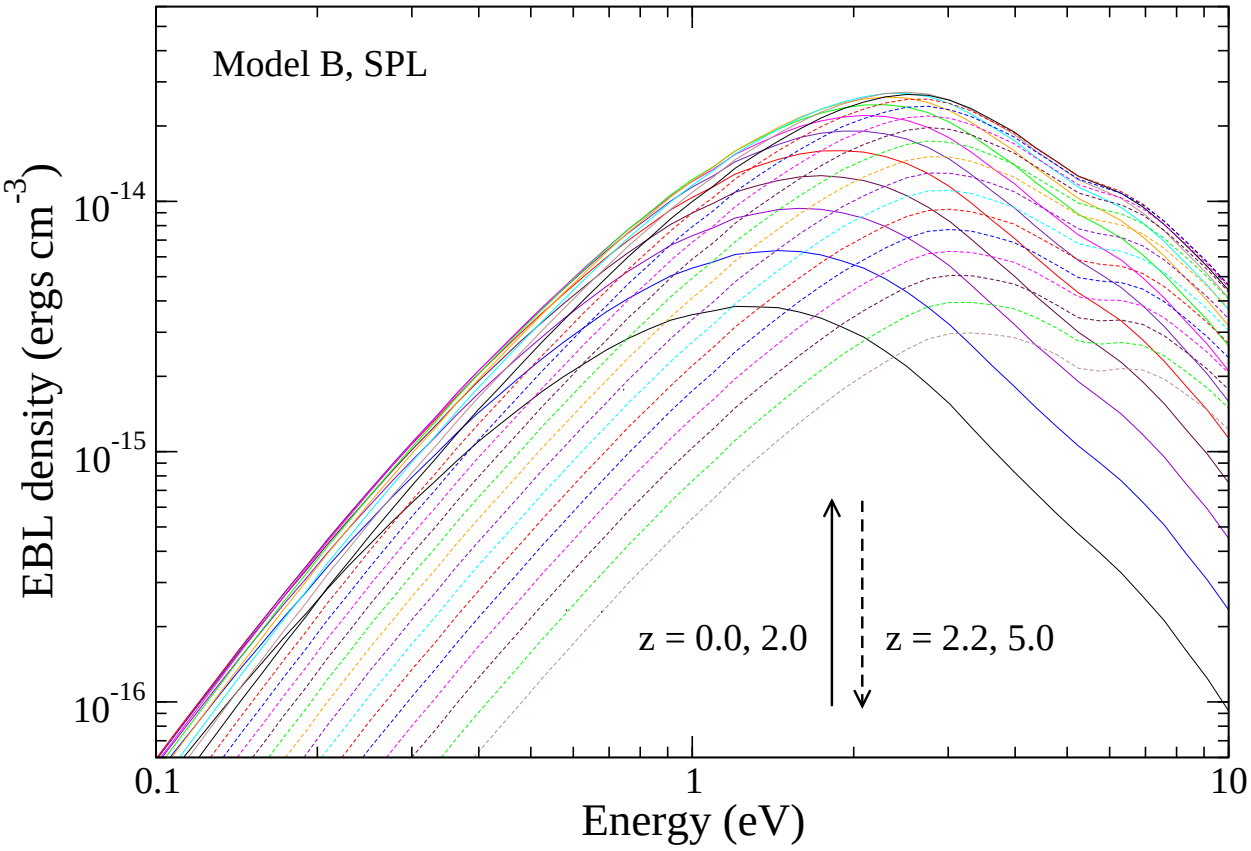


Fig. 7.— Evolution of the comoving EBL energy density $\epsilon_1 u_{\epsilon_1}$ as a function of the comoving photon energy $\epsilon_1$ with redshift for our best-fit EBL model (Model B with SPL $L - M$ relation). Model (D, SPL) gives simililar results. The curves are plotted for $z = 0$–5 with 0.2 interval. The density increases first and then decreases as indicated by the solid and dashed arrows.

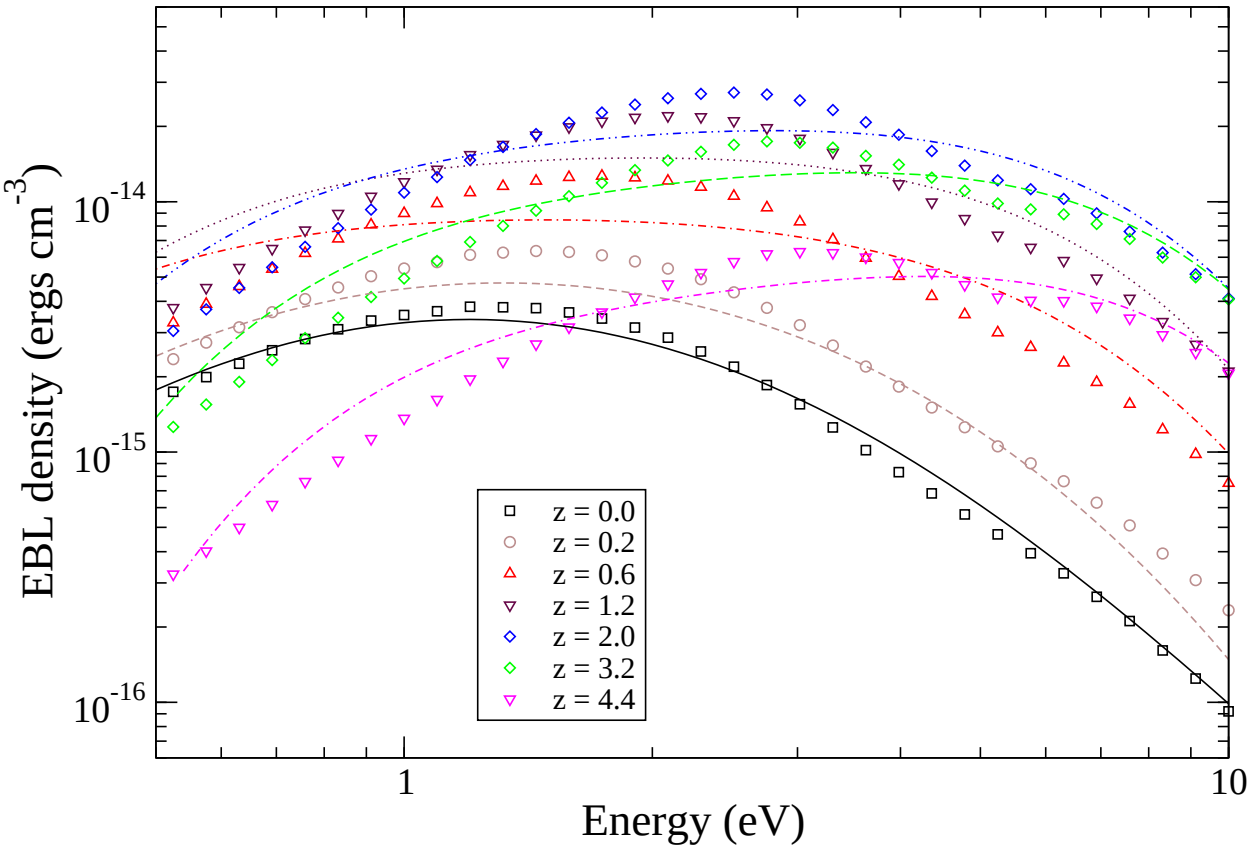


Fig. 8.— Fits (smooth lines) to an evolving EBL energy density $\epsilon_1 u_{\epsilon_1}$ (points) as a function of the comoving frame photon energy $\epsilon_1$ at different redshifts for Model (B, SPL). The fit function is given in equation (16).

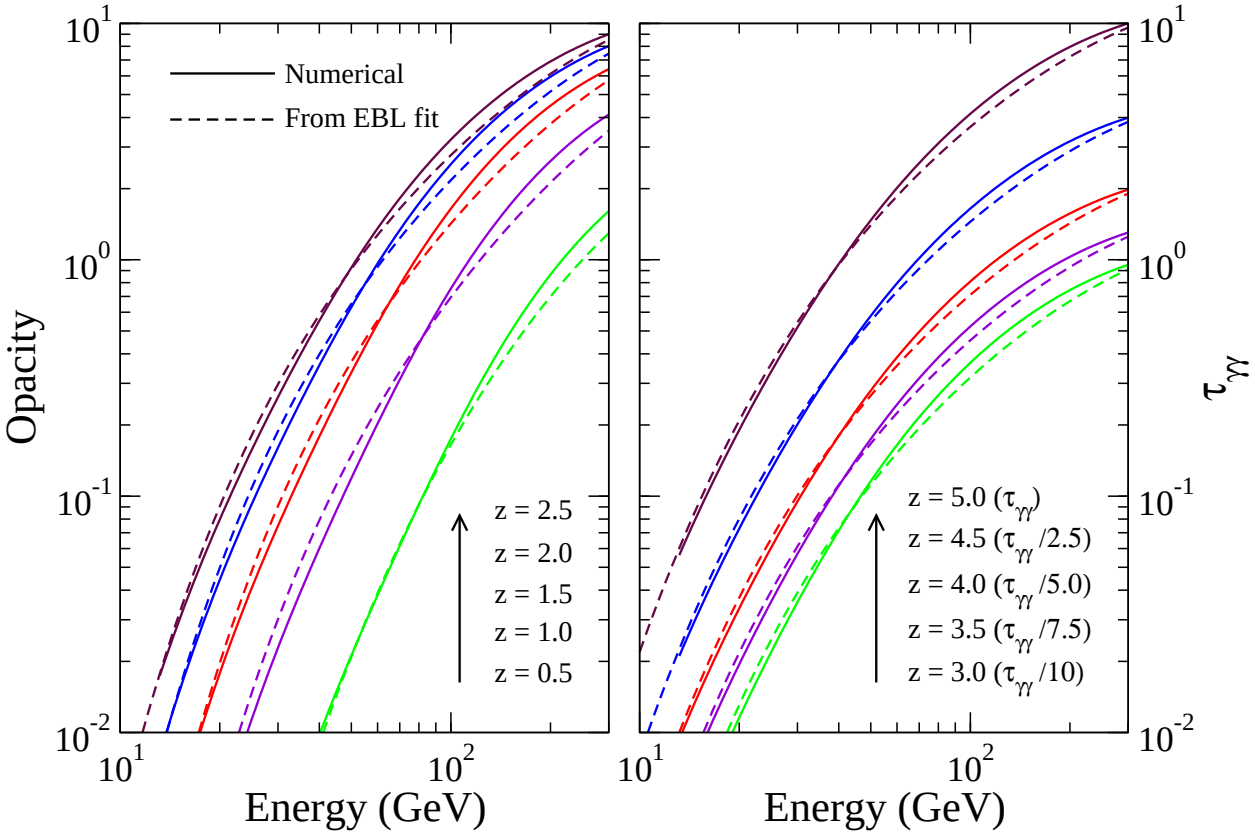


Fig. 9.— Gamma-ray opacity of the universe at different redshifts (*Left panel:* 0.5–2.5, *Right panel: 3.0–5.0*) and energies as plotted here. The solid and dashed lines correspond to the exact calculation and calculation using the fit to the EBL in equation 16, respectively. We rescaled $\tau_{\gamma\gamma}$ in the *Right panel* to separate diferent curves. The numerical values for the exact calculation are also listed in Table 1.

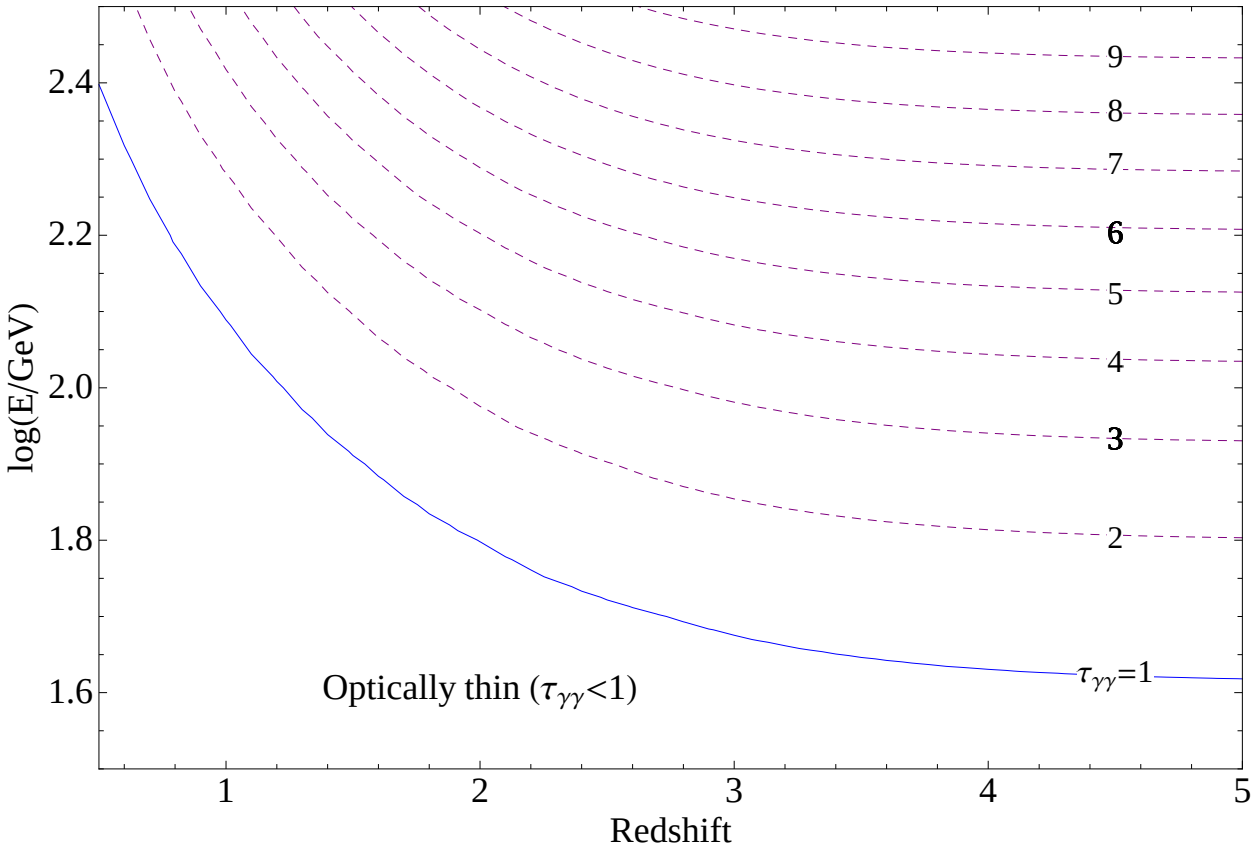


Fig. 10.— Gamma ray opacity contrours in the $E - z$ plane using the EBL fit in equation (16). The $\tau_{\gamma\gamma} = 1$ contour plotted here is known as the Fazio-Stecker relation (Fazio & Stecker 1970) and represents a $\gamma$-ray horizon of the universe.

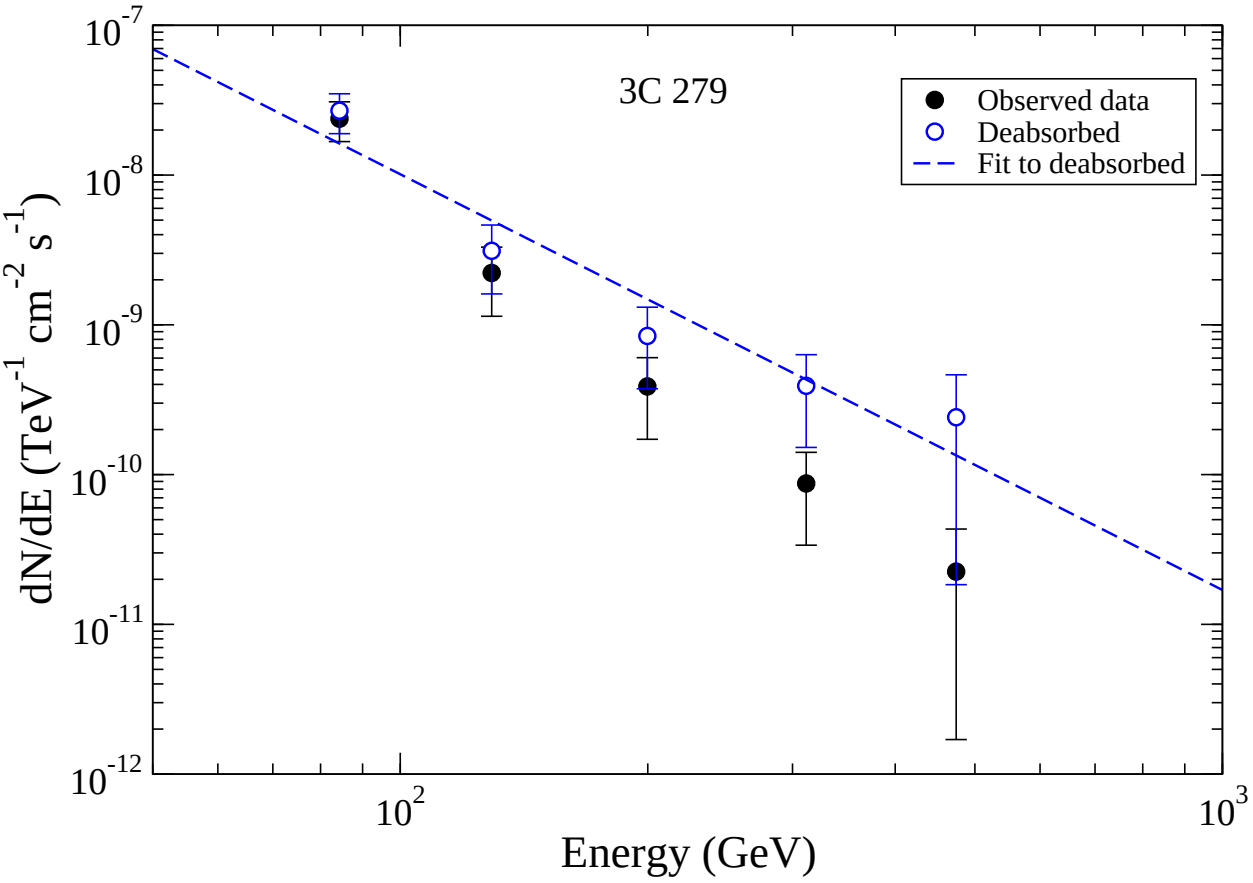


Fig. 11.— High-energy $\gamma$-ray flux from the furthest known ($z = 0.536$) blazar 3C 279 as measured by MAGIC (filled circles with errorbars. We use our EBL Model B, SPL to estimate (deabsorb) the source flux (open circles with errorbars) by multiplying the observed data points with $\exp(\tau_{\gamma\gamma})$. The dashed line is a power-law fit $dN/dE \propto E^{-\Gamma}$ to the deabsrbed data points resulting in a spectral index $\Gamma = 2.8$.